Quarterly Journal of the Royal Meteorological Society *Q. J. R. Meteorol. Soc.* 142: 2244–2255, July 2016 B DOI:10.1002/qj.2814

RMetS
Royal Meteorological Society

A case-study of a monsoon low that formed over the sea and intensified over land as seen in ECMWF analyses

Gerard Kilroy,[a]* Roger K. Smith,[a] Michael T. Montgomery,[b] Billy Lynch[c] and Craig Earl-Spurr[c]
[a]*Meteorological Institute, Ludwig-Maximilians University of Munich, Germany*
[b]*Department of Meteorology, Naval Postgraduate School, Monterey, CA, USA*
[c]*Bureau of Meteorology, Darwin, Australia*

*Correspondence to: G. Kilroy, Meteorological Institute, Ludwig-Maximilians University of Munich, Theresienstrasse 37, 80333 Munich, Germany. E-mail: gerard.kilroy@lmu.de

A case-study is presented of a tropical low that formed near Darwin, Australia, during the monsoon and subsequently intensified over land. The study is based on European Centre for Medium-range Weather Forecast (ECMWF) analyses. Interpretations of the formation over the sea are given in terms of vorticity dynamics. The thermodynamic support for the intensification and maintenance of the low over land is investigated also. The analyses indicate that the intensification of the low depends on repeated bursts of deep convection occurring near the centre of the circulation that promote the further concentration of vorticity near the centre. This concentration of vorticity increases the local circulation about the centre, which amounts to increasing the local tangential wind speed and, through approximate gradient wind balance above the boundary layer, to a lowering of the central pressure. It is found that the horizontal transport of moisture into a mesoscale column centred on the low is approximately equal to the moisture lost by precipitation, so that total precipitable water levels are not rapidly depleted over land. While the contribution to the overall moisture budget by surface fluxes is comparatively small, these fluxes are necessary to maintain conditionally unstable conditions near the vortex centre so that deep convective bursts can continue to occur there, even when the system is located far inland.

Key Words: tropical depressions; tropical lows; tropical cyclogenesis; monsoon

Received 15 October 2015; Revised 29 February 2016; Accepted 29 March 2016; Published online in Wiley Online Library 8 June 2016

1. Introduction

During the Australian 'Wet Season' (November–April) a trough of low pressure lies south of the Equator with the trough axis coinciding approximately with the 'monsoon shear line'. The latter separates westerly flow to the north from easterly flow to the south (McBride and Keenan, 1982). Early in the wet season, the trough and shear line lie over the seas to the north of Australia, but later they may move southwards. The latitude of the trough axis may vary considerably with longitude at any one time and parts may lie over the continent. It is typical for low pressure systems to develop at spatial intervals along the trough. Since water temperatures to the north of Australia can be as high as 30 °C, lows that form over the ocean frequently develop into tropical cyclones. However, sometimes lows may form and intensify while remaining over land and, like tropical cyclones, these systems pose a challenge to forecasters in the region. A pioneering and insightful analysis of tropical cyclogenesis in the Australian region is provided by McBride and Keenan (1982).

While much is now known about the structure of tropical cyclones and the mechanisms by which they intensify (e.g. Montgomery and Smith, 2014; Smith and Montgomery, 2015), rather less is known about the structure of intensifying tropical lows over land as well as the role of deep convection in their maintenance. Even though the lows form over a region with relatively sparse conventional data coverage, current numerical forecast models such as that of the European Centre for Medium-range Weather Forecasts (ECMWF) sometimes show considerable skill in predicting both their formation and evolution. For this reason it is instructive to analyze such forecasts, or better still the analyses that are based in part on the previous forecast and in part on available observations.

As a step in this direction, Smith *et al.* (2015) examined three lows that formed in the Australian monsoon during January 2013 on the basis of ECMWF analyses. All three lows formed on the monsoon shear line and two of them became tropical cyclones. Interpretations of genesis were given in terms of vorticity dynamics and applied equally to one initial development over land as well as two over the sea. It was found that the intensification of a low requires repeated bursts of deep convection near the centre of the gyre to promote the further concentration of vorticity near the centre. This vorticity concentration increases the local circulation about the centre, which amounts to increasing the local tangential wind speed and, through approximate gradient wind balance above the boundary layer, to a lowering of the central pressure.

1.1. Two scientific questions

Two important scientific questions concerning the formation and intensification of tropical lows over land were raised by Smith *et al.* (2015). One question is whether their intensification is fundamentally different from that of tropical cyclones over the sea. Another question is whether the marsupial paradigm proposed by Dunkerton *et al.* (2009) is useful in understanding the formation of tropical cyclones in the monsoon regime of northern Australia, and indeed for monsoon depressions over land.

The marsupial paradigm refers to the nurturing role of a tropical wave in the formation of tropical depressions. The hybrid wave-vortex structure was likened to the development of a marsupial infant in its mother's pouch. By analogy, a juvenile proto-vortex is carried along by its parent wave until the proto-vortex is strengthened into a self-sustaining entity. For tropical storms developing within tropical waves, the recirculating flow in the wave's critical layer corresponds to the 'pouch' where the wave and mean-flow speeds are similar. The centre of the pouch is defined as the intersection of the trough axis and the critical latitude,* which is oriented parallel to the easterly jet. Storm formation occurs near this so-called sweet spot.

Support for the relevance of the marsupial paradigm to tropical low formation in the monsoon regime was found in the three lows investigated by Smith *et al.* (2015). They showed that for these cases, low formation occurred only in regions where the Okubo–Weiss parameter was large and positive near the centre of the nascent vortex, indicating a minimal detrimental effect of shearing deformation on the vortex (Rozoff *et al.*, 2006; Montgomery *et al.*, 2012). However, a more complete answer to the latter question calls for an investigation of the supply of moisture to sustain deep convection, particularly in the case of lows that form and/or intensify over land.

1.2. Thermodynamic support for intensification over land

Kaplan and DeMaria (1995) found that, when a tropical low moves inland and is cut off from the large heat fluxes from the underlying ocean, it rapidly decays with an exponential time constant of around 10 h. There are some exceptions to this behaviour with certain types of terrain being less detrimental to storm decay than others. Shen *et al.* (2002) found that large heat fluxes over swampy terrain leads to redevelopment over land, and this terrain also provides larger surface fluxes of moisture than the arid desert terrain of Northern Australia.

Emanuel *et al.* (2008) sought to explain the redevelopment of warm-core cyclones over land in Northern Australia using an axisymmetric atmospheric model coupled to a simple model of the upper ocean. The basis of the model is presented by Emanuel (1995) and is designed around the assumption of slantwise convective neutrality along surfaces of constant absolute angular momentum. They found that warm-core cyclones can indeed intensify when the underlying soil is sufficiently warm and wet and the system is maintained by sensible heat and moisture (latent heat) transfer from the soil. In this model, landfall is simulated by setting the surface enthalpy flux coefficient to a value that diminishes with land elevation (Emanuel *et al.*, 2004). They conclude that, when the storms are sufficiently isolated from their oceanic source of moisture, the rainfall they produce is insufficient to keep the soil wet enough to transfer significant quantities of heat,† and the storms then decay rapidly.

The strong focus on surface fluxes over land has no doubt been influenced by the WISHE paradigm for tropical cyclone intensification, which invokes a multi-step feedback process between surface enthalpy fluxes and a spin-up of the tangential winds. This widely accepted feedback mechanism has been shown to be non-essential in explaining the intensification of tropical cyclones (Montgomery *et al.*, 2009, 2014).

Evans *et al.* (2011) performed numerical simulations of tropical cyclone *Erin* (2007), a storm that made landfall from the Gulf of Mexico and underwent re-intensification over the central United States. They found that the Emanuel *et al.* (2008) along-track tropical cyclone rainfall feedback mechanism to be 'of minimal importance to the evolution of the vortex'. They concluded that 'the final intensity of the simulated (and presumably observed) vortex appears to be closely linked to the maintenance of boundary-layer moisture over pre-existing near-climatological soil moisture content along the track of the vortex and well above climatological soil moisture content'. They noted that 'variations in soil moisture content result in impacts upon the boundary-layer thermodynamic environment via boundary-layer mixing. Greater soil moisture content results in weaker mixing, a shallower boundary layer, and greater moisture and instability. Differences in the intensity of convection that develops and its accompanying latent heat release aloft result in greater warm-core development and surface vortex intensification within the simulations featuring greater soil moisture content'.

Sharkov *et al.* (2012) sought to determine the necessary amount total precipitable water (TPW) for genesis in the surrounding atmosphere over the ocean. They found that there is a critical value (60 kg m^{-2}) of TPW over a region surrounding the tropical cyclone so that it persists longer than 24 h. Interestingly, Emanuel *et al.* (2008) did not consider the horizontal transport of moisture into the vortex, a potentially large source of moisture that may help sustain the system, even though some degree of surface fluxes are indeed necessary for a vortex to be able to deepen (e.g. Malkus and Riehl, 1960). For one thing, such moisture fluxes are required to maintain conditional instability and thereby to sustain deep convection within the vortex circulation.

1.3. The present study

In this article we examine a further case of the formation and structure of a tropical low in the Australian monsoon regime. As in Smith *et al.* (2015), the study is based largely on ECMWF analyses. Unlike in the cases studied by Smith *et al.* (2015), the low intensified as it moved southwards over the land. Here we study the life cycle of the disturbance prior to its extratropical transition. The objective is to provide a vorticity perspective of genesis and an analysis of the moisture supply necessary to support intensification.

The article is organized as follows. First, in section 2 we present details of the datasets on which our analyses are based. A description of the evolution of the system from a forecaster's perspective is given in section 3. In section 4 we introduce the necessary diagnostic tools which we use to explain the formation and intensification of the low. In section 5 we examine the genesis of the low and its evolution after landfall. In section 6 we present the conclusions.

2. Datasets

The ECMWF analyses used for this study are available at the surface and at 25 pressure levels between 1000 and 1 mb. They cover the domain from 100°E to 160°E, from the Equator to 30°S, and have a horizontal grid spacing of 0.125°. The case-study is based largely on selected kinematic and thermodynamical fields extracted from these analyses, supplemented by geostationary satellite imagery from the Japanese Meteorological Satellite (MTSAT). The analyses, which are obtained from a global 4D-Var analysis and prediction system, are considered by forecasters to be as good as any available.

*The critical latitude on a particular pressure surface is defined by the locus of points satisfying $U = c_{px}$, where cpx denotes the zonal phase speed of the wave and U denotes the local zonal wind.

†Emanuel *et al.* (2008) do not make a distinction between sensible and latent heat.

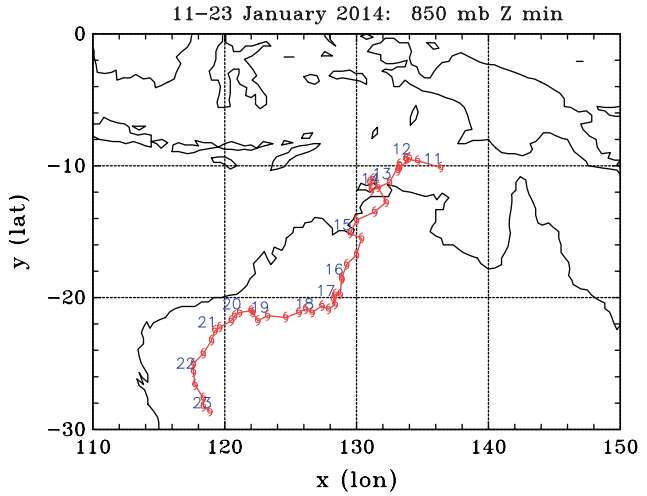

Figure 1. Track of the tropical low from 11 to 23 January 2014. Positions at 0000 UTC (shown by date) of the minimum geopotential at 850 mb are indicated by cyclone symbols every 6 h.

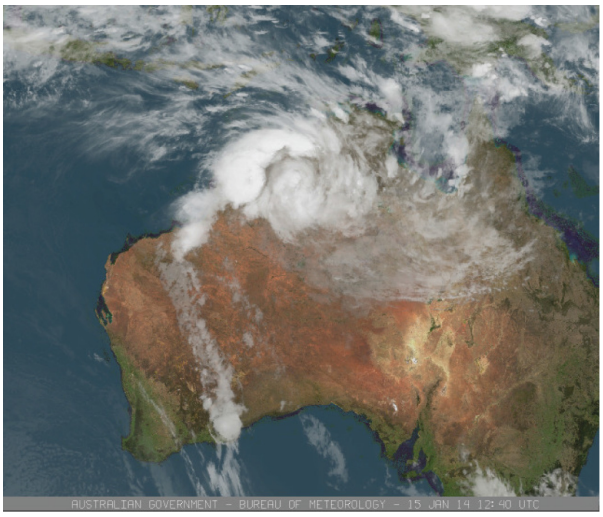

Figure 2. Visible satellite image on 15 January 2014 at 1200:40 UTC.

3. Low evolution from a forecaster's perspective

During the early hours of 11 January 2014, convection within a deepening monsoon trough was strongest over the Arafura Sea to the north of the Northern Territory's 'Top End' and west of a previously identified weak circulation near Cape York Peninsula, south of New Guinea. This region of strong convection was identified also as the region of strongest local vertical vorticity. Scatterometry[‡] later in the day indicated that a new low had formed in this region. This new low is the focus of our study. The track of this low, as determined by the minimum geopotential at 850 mb, is shown in Figure 1.

The environment was broadly favourable with a deep layer of moist air and a deep (up to 500 mb) and almost upright system (some overlap of the 850 and 500 mb centres). Deep vertical shear was moderate (about 10 m s^{-1} from the east), but not hugely detrimental. From 0000 UTC[§] on 11 January, pressure falls within the monsoon trough were of the order of 3 mb day^{-1}, although some locations were measuring 4–6 mb day^{-1}. The low remained poorly defined within the monsoon trough with a large uncertainty in its position until on 12 January when persistent convection began to develop. Up until this point, persistent convection near the low was almost non-existent. Overnight of 12 January and into 13 January, the low tracked west to north of Cobourg Peninsula, about 300 km northeast of Darwin, with central pressures falling below 1000 mb. Thunderstorms finally started flaring near the circulation centre during this time and at 0600 UTC on 13 January a Dvorak initial classification (Current Intensity (CI) 1.0) was assigned by the Darwin Tropical Cyclone Warning Centre.

Model guidance had been mixed up to this point. The ACCESS suite (Australian Community Climate and Earth-System Simulator) was predicting the most intense storm, whereas other models including the ECMWF model were not indicating intensification. ECMWF was also indicating a monsoon low structure with the strongest winds away from the low centre. ECMWF ensemble probabilities for a tropical storm barely exceeded 20%. All models were indicating a southwestward movement towards the Kimberley region of Western Australia, but it was a fine line between a track that moved over the Timor Sea versus a track that moved over the western Top End south of Darwin. Over time, the consensus track was shifting further east and eventually over land.

The Darwin Tropical Cyclone Warning Centre began issuing advice to the community on 13 January, with a Tropical Cyclone Watch issued at 0130 UTC for the possibility of the low developing into a tropical cyclone in 24–48 h. However, overnight on 13 January the low took a southerly track and, based on an analysis of surface observations, crossed the coast just after 0000 UTC on 14 January, about 100 km east of Darwin, with a CI of 1.0. The mid-level centre, as tracked on radar, was now displaced west of the low-level centre indicating the effects of easterly vertical shear.

Although the consensus track was over land, the uncertainty still allowed for movement into the Timor Sea and subsequent intensification. At 0430 UTC on 14 January the Tropical Cyclone Watch was upgraded to a Tropical Cyclone Warning, for the possibility of a tropical cyclone forming in the southern Timor Sea within 24 h. However, as the low continued to track southwestward over land, the time available to move over water and intensify diminished and at 2230 UTC on 14 January the Tropical Cyclone Warning was cancelled.

Heavy rain developed in the Darwin region following the passage of the low with reports of flash flooding. The heaviest 24 h rainfall during this event was 205.6 mm recorded at Elizabeth Valley (40 km southeast of Darwin) in the 24 h period to 2330 UTC on 14 January. Figure 2 shows a satellite image of the system on 15 January at 1240 UTC. The widespread rainfall continued as the low tracked across the western Top End and moved south on 15 January. Despite being over land, the system continued to deepen as it moved southward over the Tanami Desert and it was located favourably beneath the upper-level ridge.

On 17 January the system had a central pressure of 992 mb and headed in a westerly direction across the interior of Western Australia and into the Pilbara region, passing southeast of Marble Bar on 20 January. The system reached its lowest central pressure of 989 mb on 21 January and then rapidly weakened as it recurved to the southeast before being captured in the midlatitude westerly airstream. The low maintained remarkable structure while over land until it was captured by this westerly airstream.

4. Vorticity and Okubo–Weiss diagnostics

In this section we first introduce the necessary diagnostic tools which we use to explain the formation and intensification of the low. Smith *et al.* (2015) showed that insight into the monsoon and the low pressure systems that form within could be obtained by an analysis of the vorticity field and its time evolution. In pressure coordinates, the vorticity tendency equation has a particularly concise form in which the local tendency of absolute vorticity ζ_a can be written as the horizontal divergence of a horizontal flux (Haynes and McIntyre, 1987; Raymond and López Carillo, 2011;

[‡]Scatterometry is a method for determining near-surface wind speed and direction over oceans and consists of a satellite-borne microwave radar sensor used to measure reflection or scattering effects produced by wind waves.
[§]Universal Time Coordinated. Note that local time is 9.5 h ahead of UTC.

Tory *et al.*, 2012; Raymond *et al.*, 2014), i.e.

$$\frac{\partial \zeta_a}{\partial t} = -\nabla_h \cdot \mathbf{F}_{\zeta_a}, \qquad (1)$$

where $\mathbf{F}_{\zeta_a} = \mathbf{F}_{af} + \mathbf{F}_{naf}$, with $\mathbf{F}_{af} = \mathbf{u}_h \zeta_a$, and $\mathbf{F}_{naf} = -\zeta_h \omega + \mathbf{k} \wedge \mathbf{F}_{fri}$. Here $\mathbf{u}_h$ is the horizontal velocity vector, ζ_h is the horizontal component of vorticity, ω is the material derivative of pressure and plays the role of 'vertical velocity' in pressure coordinates, $\mathbf{F}_{fri}$ is the horizontal force per unit mass due to molecular effects and subgrid-scale eddy momentum fluxes, and $\mathbf{k}$ is a unit vector in the vertical. More details about the benefits of analysing vertical vorticity in this form are given in Smith *et al.* (2015).

While useful in characterizing local rotation, vertical vorticity may be associated with regions of strong horizontal shear deformation, which is detrimental to the formation of concentrated vortices. Favourable regions for vortex formation are those where the vorticity is dominated by pure rotation. Dunkerton *et al.* (2009) used depictions of the Okubo–Weiss (OW) parameter (Appendix in Smith *et al.*, 2015) to highlight regions within the broadscale flow that tend to be most immune to horizontal shear deformation, i.e. regions where the flow is rotationally dominant. These are regions where convectively generated patches of vertical vorticity are most capable of congealing to form a monopole structure. We examine such diagnostics here also.

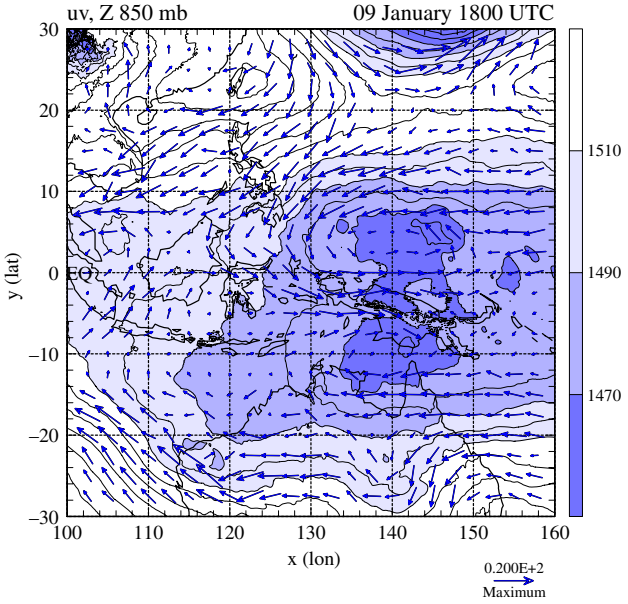

Figure 3. Isopleths of 850 mb geopotential height for an extended domain on 9 January 2014 at 1800 UTC. Shading indicates weak low pressure systems each side of the Equator near 140°E. The contour interval is 10 m, with shaded regions as given in scale bar. Wind vectors at 850 mb are also shown.

5. Low development as seen in the ECMWF analyses

We divide our analysis of the low into two time periods: the early period of formation over the sea, where we examine the initial intensification of the low from a vorticity perspective, and the period of subsequent intensification over land, where we focus on the moisture supply needed to support the intensification process. We take landfall to be at 0600 UTC on 14 January, when in the ECMWF analyses (Figure 1) the minimum geopotential of the system crossed the coast.

5.1. *Formation*

Figure 3 shows geopotential heights at 850 mb at 1800 UTC on 9 January for a region north and south of the Equator. A notable feature is a region of low geopotential straddling the Equator with local minima in each hemisphere. This structure is characteristic of an equatorially trapped $n = 1$ Rossby wave (ER wave). In animations of these fields (not shown), the two lows move polewards and westwards over 10 days, with the Northern Hemisphere low remaining weaker than the Southern Hemisphere one. Consistent also with an ER wave structure is a band of strong westerlies at the Equator known as a westerly wind burst.

The Southern Hemisphere low of the ER wave appears to be the precursor disturbance leading to the low of interest here and presumably provided a favourable 'pouch' in which the low was able to intensify. Tropical cyclogenesis within ER waves is described in detail by Molinari *et al.* (2007).

Figure 4 shows the wind structure at 850 mb together with wind vectors, contours of the zonal wind component and contours of geopotential height at 0000 UTC from 9 to 14 January 2014. On 9 January there is a region of locally strong westerlies near Papua New Guinea and a weak cyclonic gyre south of Papua New Guinea within a larger area of low geopotential heights, but the easterly winds to the south of the island in the belt from 130 to 160°E are relatively light. In the days that follow, the easterlies strengthen across northern Australia as an anticyclone moves eastwards to the south of the continent. The synoptic situation is very similar to that for tropical cyclone *Narelle* (2013) described by Smith *et al.* (2015). There is a large expansion also in the area of the stronger monsoon westerlies ($>10\,m\,s^{-1}$) between the Equator and 10°S. Moreover, the circulation within the gyre increases and there is an accompanying lowering of the 850 mb geopotential heights near the centre of the gyre. It was at 0130 UTC on 13 January (shortly after the time shown in Figure 4(e)) when a Tropical Cyclone Watch was issued for the possibility of the low developing into a tropical cyclone in 24–48 h. In Australia, bursts of monsoon activity are often associated with the Madden–Julian Oscillation (MJO), although the Australian Bureau of Meteorology announced on 7 January that the 'MJO signal has been weak or indiscernible since late December. As the signal has been weak, it is unlikely to have had a significant influence on tropical weather during this period. Forecasts of the MJO indicate that it is most likely to remain weak or indiscernible for at least another week'.

Figure 5 shows the magnitude of the mean vertical wind shear[¶] between 850 and 200 mb averaged over columns 2° × 2°, 4° × 4°, and 6° × 6° centred on the location of the minimum geopotential at 850 mb together with the maximum wind speed at 850 mb within the 2° × 2° column. The latter serves as a measure of the system intensity. Until about 0000 UTC on 13 January, there was moderate vertical shear ($\approx 10\,m\,s^{-1}$) and the low did not intensify. Thereafter the vertical shear decreased in magnitude and the low intensified. The maximum wind speed nearly trebled in strength from about $10\,m\,s^{-1}$ at 0000 UTC on 13 January to nearly $30\,m\,s^{-1}$ on 16 January. Note that the average values of the shear over the three different-sized columns is very similar. From 0600 UTC 14 January, the system was over land. It is not possible to conclude from the analyses that the decrease in vertical shear led to the intensification or whether the intensification itself led to the reduction in shear. Compared to tropical cyclone *Narelle* described in Smith *et al.* (2015), the low here suffered larger magnitudes of vertical shear during its formation (the shear in the *Narelle* case was under $5\,m\,s^{-1}$) for most of the genesis period).

5.2. *A vorticity perspective of formation and evolution*

A vorticity perspective of the foregoing development is illustrated in Figure 6(a, c, e), which shows the vertical component of

[¶]The shear is characterized here by the magnitude of the vector velocity difference between the two levels, averaged over the column. We compute first the local vector velocity difference and then compute the average over the box. Because of the linearity of the shear vector calculation, the method is equivalent to computing the vector shear from the difference in the areal average velocity at the two levels. This is equivalent to the method adopted by DeMaria and Kaplan (1994, p. 213) as a basis for their Statistical Hurricane Intensity Prediction Scheme (SHIPS).

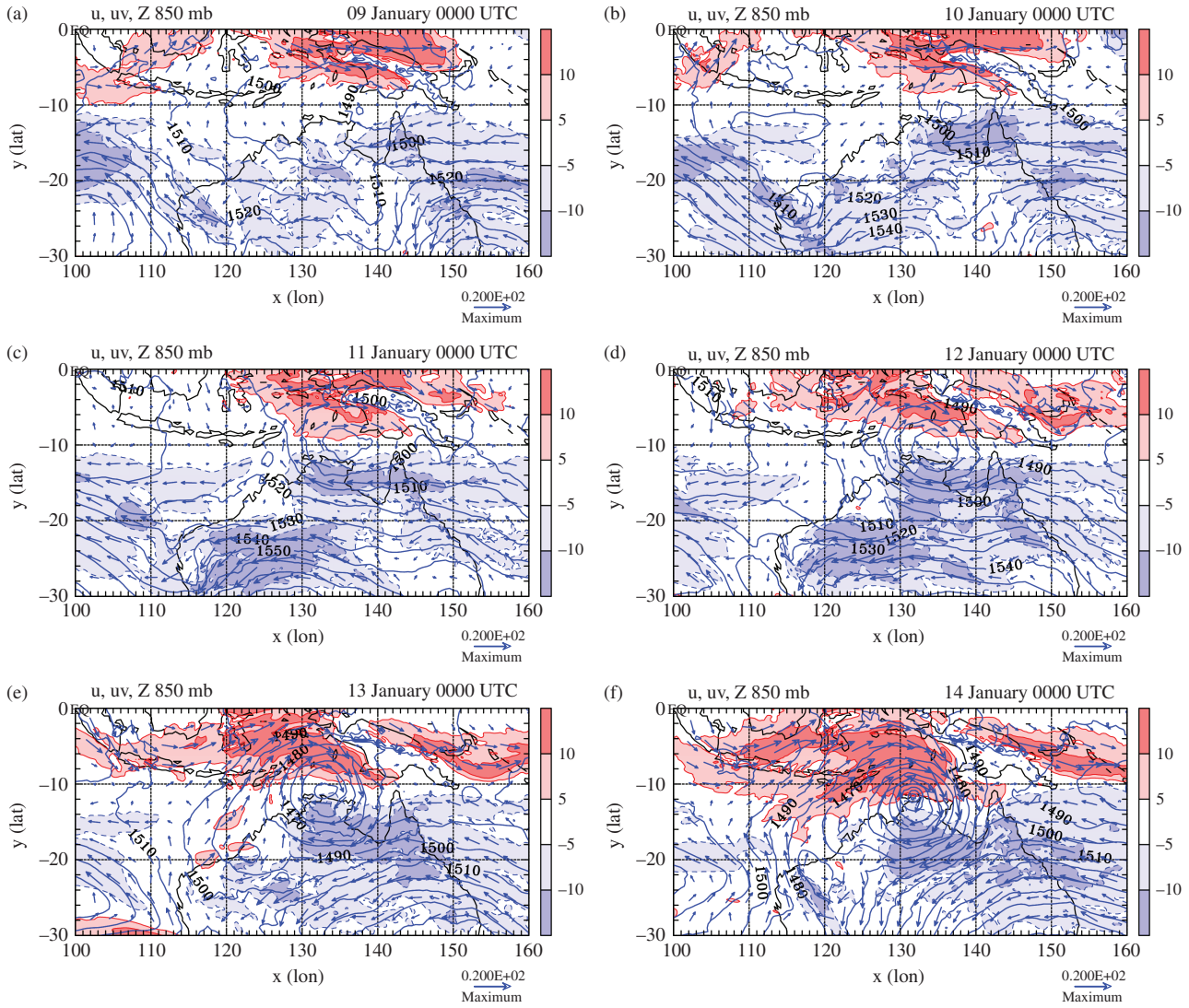

Figure 4. Wind vectors at 850 mb together with contours of the zonal wind component (solid contours positive, dashed contours negative) and of geopotential height (blue, interval 10 m) at 0000 UTC on (a) 9 January, (b) 10 January, (c) 11 January, (d) 12 January, (e) 13 January and (f) 14 January 2014 illustrating the formation and intensification of the low. Westerly wind components greater than 5 (10) m s^{-1} are shaded pink (red). Easterly winds greater than 5 (10) m s^{-1} in magnitude are shaded light blue (darker blue). Wind vectors should be compared to the reference vector (20 m s^{-1}) at the bottom right of each panel.

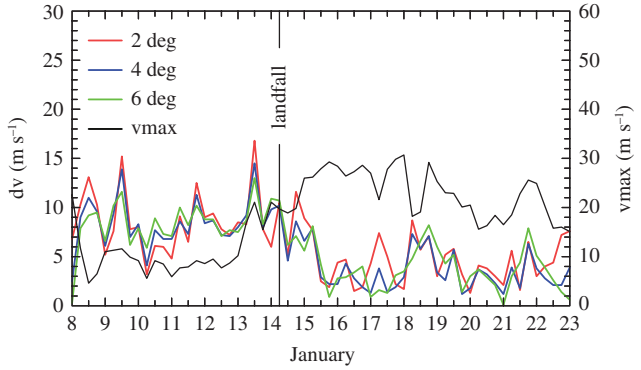

Figure 5. Mean vertical wind shear, characterized by the magnitude of the vector velocity difference between 850 and 200 mb, averaged over lat–long columns 2° × 2°, 4° × 4°, and 6° × 6° centred on the location of the minimum geopotential at 850 mb, and maximum wind speed at 850 mb (black line) within the 2° × 2° column.

absolute vorticity together with the corresponding wind vectors and the contours of geopotential height at 850 mb. At 0000 UTC on 9 January, the most prominent feature in the absolute vorticity is the broad region of elevated positive values[‖] over and south of Papua New Guinea. There is a weak circulation centred over the ocean south of Papua New Guinea at latitude 10°S, although the centre of the circulation has only sparse patches of enhanced vertical vorticity (values above 10^{-4} s^{-1}) at this time. The broad circulation encompasses also a region of low 850 mb geopotential heights. By 0000 UTC on 11 January, the clump of absolute vorticity near the circulation has increased significantly in strength and areal extent, the recirculating winds show a commensurate increase in strength and the geopotential has lowered further. The vortex has moved to the west by this time, but has remained at latitude 10°S. By 0000 UTC on 13 January, the circulation has strengthened and geopotential heights have dropped further. At this stage the system is relatively large in size with closed contours of geopotential heights about 10° longitude in diameter.[**] The size of this low is huge when compared to tropical cyclone *Tracy* (1974), which devastated Darwin on Christmas Day (Davidson, 2010 and references therein). The radius of gales in the case of *Tracy* was merely 50 km.

Figure 6(b, d, f) shows the distribution of the OW parameter at the 850 mb level at 0000 UTC on the 9, 11 and 13 January. The major feature of the OW field is the coherent region of positive

[‖]The sign of the vertical vorticity is reversed for similarity to Northern Hemisphere cases.

[**]Typically, forecasters describe storm size in terms of the outer core radius of gales (radius of the 17 m s^{-1} total winds) at a height of 10 m. In this case it is difficult to describe size in the conventional way as the system is embedded in a large region of background gale force winds near the surface, with the region of gales extending from 120° to 140°E (not shown).

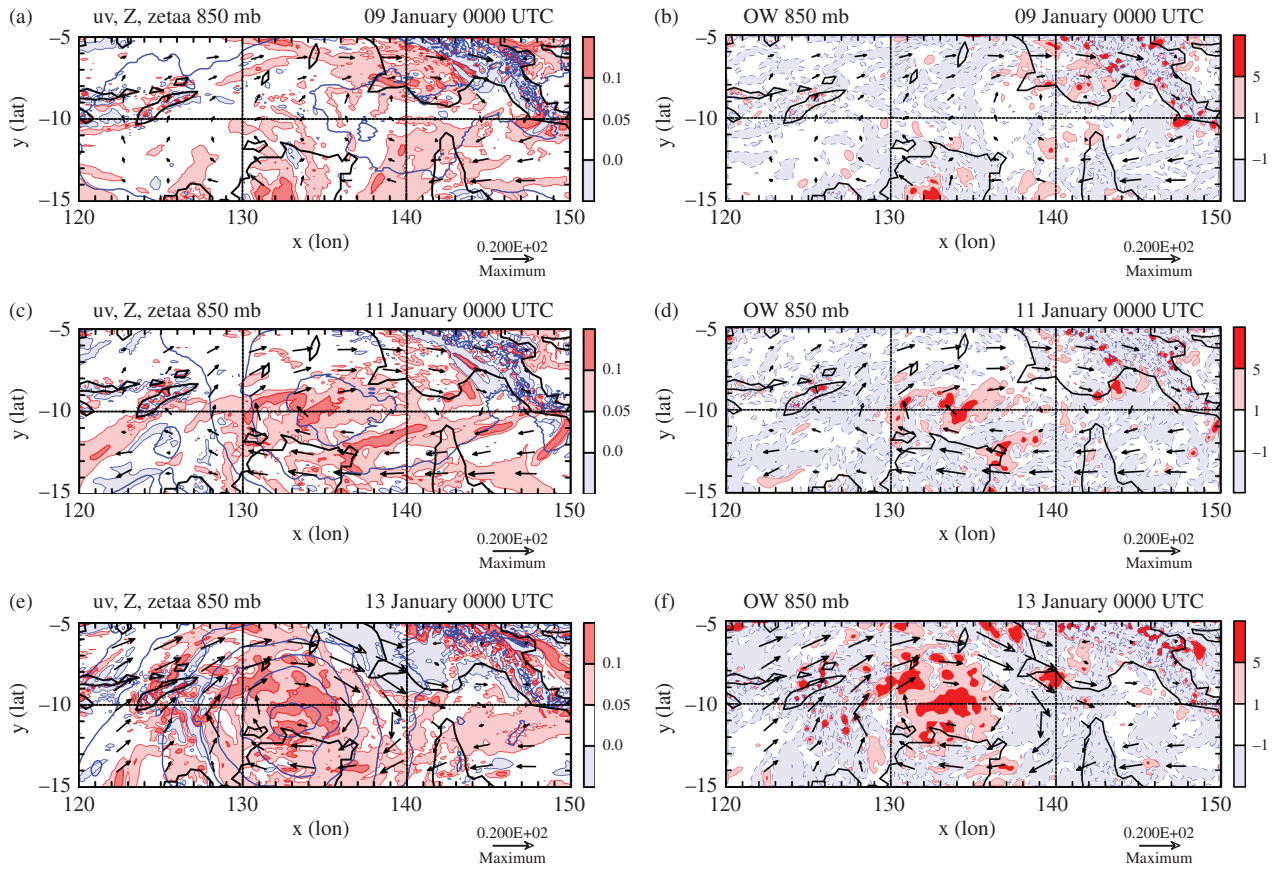

Figure 6. (a, c, e) Wind vectors at 850 mb together with contours of the absolute vorticity (colour shaded) and geopotential height (thick blue contours, interval 10 m) at 0000 UTC on (a) 9 January, (c) 11 January, and (e) 13 January 2014 illustrating the formation of the low. Absolute vorticity shading is as shown on the label bar multiplied by 10^{-3} s^{-1}. Cyclonic vorticity is positive (red/pink shading), anticyclonic is negative (light blue shading). (b, d, f) Contours of the Okubo–Weiss (OW) parameter (shading) at 0000 UTC on (b) 9 January, (d) 11 January, and (f) 13 January 2014 illustrating environment during the formation of the low. OW shading is as shown on the label bar multiplied by 10^{-8} s^{-2}. Wind vectors should be compared to the reference vector (20 m s^{-1}) at the bottom right of each panel.

values within the nascent vortex circulation centred near 10°S, while elsewhere in this flow, positive OW values are relatively small in scale. This major OW feature is coherent up to 700 mb (not shown), and is one factor, at least, indicating that the vortex has the potential for further development. However, as shown in Figure 5, there is moderate vertical shear at these times, a factor that may have prohibited development. On 11 January the strongest patch of positive OW is located west of the vortex centre. During the next two days the areal extent of positive OW increases around this strong patch and the emergent vortex itself centres on this patch. The strength of the patch increases also during the three-day time period.

As a step towards understanding the role of deep convection in the spin-up of low-level vorticity, we examine next areas of strong upward velocity (vertical p-velocity $\omega < -0.5$ Pa s^{-1}: a proxy for deep convection in the model) at 500 mb as the vortex evolves. These areas are shown in Figure 7 with the horizontal wind fields at 850 mb superimposed. Figure 8 shows the corresponding fields of absolute vorticity at 850 mb with the advective flux vectors of absolute vorticity ($\mathbf{F}_{af}$) superimposed.

From 0000 UTC on 9 January until 0000 UTC on 11 January, there are broadscale regions of disorganized vertical motion in the vicinity of the vortex centre. During this time the vectors $\mathbf{F}_{af}$ indicate a flux of absolute vorticity around, and with a component towards, the centre of circulation of the nascent vortex. In particular, on 9 and 10 January there is a large flux of absolute vorticity from around southern Papua New Guinea into the circulation centre.

By 12 January the regions of strong ascent have reorganized and now form an encircling band around the nascent vortex, with little convective activity in the inner core of the system. The cyclonic absolute vorticity has become consolidated around the developing vortex circulation. On 13 and 14 January, regions of strong vertical velocity occur closer to the circulation centre. It is during these two days that the maximum wind begins to increase noticeably within the 2° × 2° column (Figure 5). Below the level of non-divergence, typically in the mid-troposphere, the upward motion leads to the low-level convergence of air, and therefore (from the flux form of the vorticity equation) to low-level convergence of absolute vorticity. In turn, this convergence leads to an amplification of the tangential wind field of the nascent vortex about the centre of circulation.

On the sub-vortex scale, there is a number of locally strong updraught cells in the model,[††] including one particularly intense cell near the centre of circulation as defined by the minimum geopotential height at 850 mb. These cells must be contributing to the convergence of absolute vorticity and material stretching of vortex tubes, equivalent to minus the divergence of the advective flux in the flux form of the vorticity equation (Eq. (1)). Recalling the material form of the vorticity equation, it follows that, as a vortex tube is stretched by an updraught, there will be a local amplification of both the vorticity and wind speed.

Figure 9 shows time–height cross-sections of various quantities averaged over square columns of 2° × 2° and 10° × 10° centred on the minimum geopotential at 850 mb. These quantities include the area-averaged vertical mass flux (approximated here as the average of $-\omega$/g) the temperature, the relative humidity, and the pseudo-equivalent potential temperature, θ_e. Shown also is a time–height cross-section of normalized circulation around the column. The time at which landfall occurs is indicated in each panel. Highlighted also is the time at which landfall occurs. Notable features of the vertical mass flux in the 2° column are the two 'bursts' apparent at 1800 UTC on 13 January and 1200 UTC on 14 January. During the two-day period from 0000 UTC on 13

[††]Of course, the cells in the model do not represent individual observed updraughts. The ECMWF model uses a convective parametrization scheme.

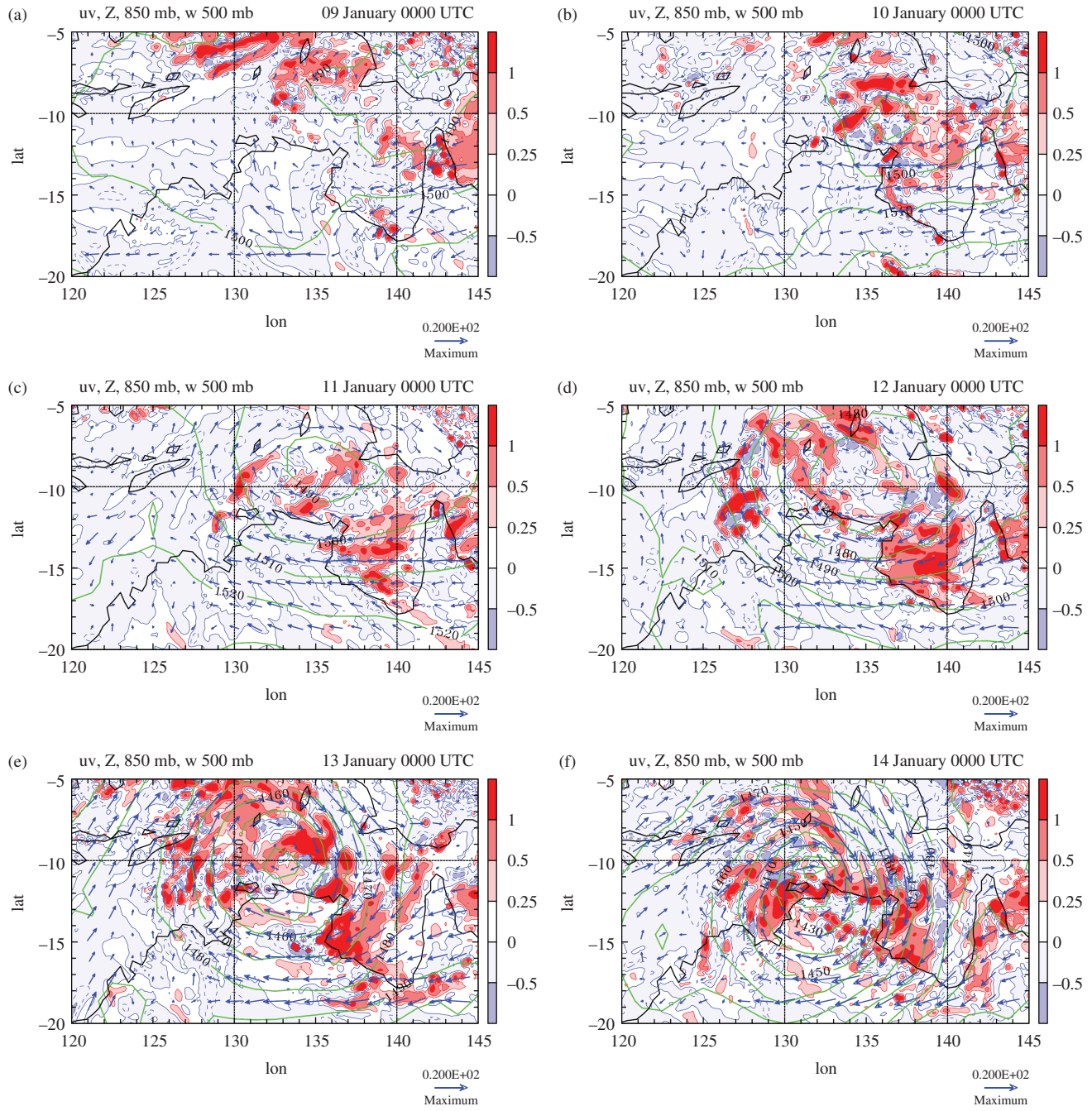

Figure 7. Wind vectors, contours of geopotential height (green, interval 10 m) together with contours of the vertical p-velocity (ω, shading, Pa s^{-1}) at 500 mb at 0000 UTC from (a) 9 January to (f) 14 January 2014, illustrating the formation. Upward vertical velocities (negative values of ω) appear as positive (red/pink), and downward velocities (positive ω) are negative (blue). Wind vectors should be compared to the reference vector (20 m s^{-1}) at the bottom right of each panel.

January to 0000 UTC on 15 January, there is a notable increase in the maximum wind speed (from 8.7 to 26.0 m s^{-1}) in the 2° column (shown in Figure 5).

Early in the evolution of the low, up to 1800 UTC on 13 January, the main convective activity occurs outside the 2° column, but inside a 10° column. The circulation around the 2° column is weak until landfall occurs and the equivalent potential temperature averaged over the square column is generally low in the mid-troposphere before landfall. The convective burst just before landfall leads to a moistening of the mid- to upper-troposphere, as seen in the relative humidity averaged over the column. These convective bursts are accompanied by a temperature increase at upper levels. However, there are periods of slightly reduced temperature, mostly below 900 mb and mostly less than 0.5 °C in magnitude. These are presumably associated with convectively induced mesoscale downdraughts.

During the mature stage of the low and beyond, from 0000 UTC on 15 January to 0000 UTC on 21 January (Figure 5), bursts of deep convective activity continue to occur in both the 2° and 10° columns (Figure 9(a, b)). These bursts are interspersed with periods of mean subsidence, which tend to be accompanied by negative temperature anomalies at low levels (pressures above 850 mb in Figure 9(c)). The mid-tropospheric minimum in θ_e continues to be progressively eroded through much of this period (Figure 9(e)) and the low-level circulation is maintained (Figure 9(f)), despite the system being over land since 0600 UTC on 14 January.

In summary, the system formed in an environment with moderately high background vertical vorticity, but also with moderate vertical wind shear. It intensified following two days of sustained deep convective bursts that occurred close to the circulation centre. During this time, the vertical shear declined. The convective bursts generated low-level convergence of absolute vorticity, which led to an amplification of the tangential wind field of the nascent vortex about the centre of circulation. The convective bursts moistened the mid- to upper-troposphere also, increasing both the relative humidity and equivalent potential temperature at these levels (shown in the next section). The

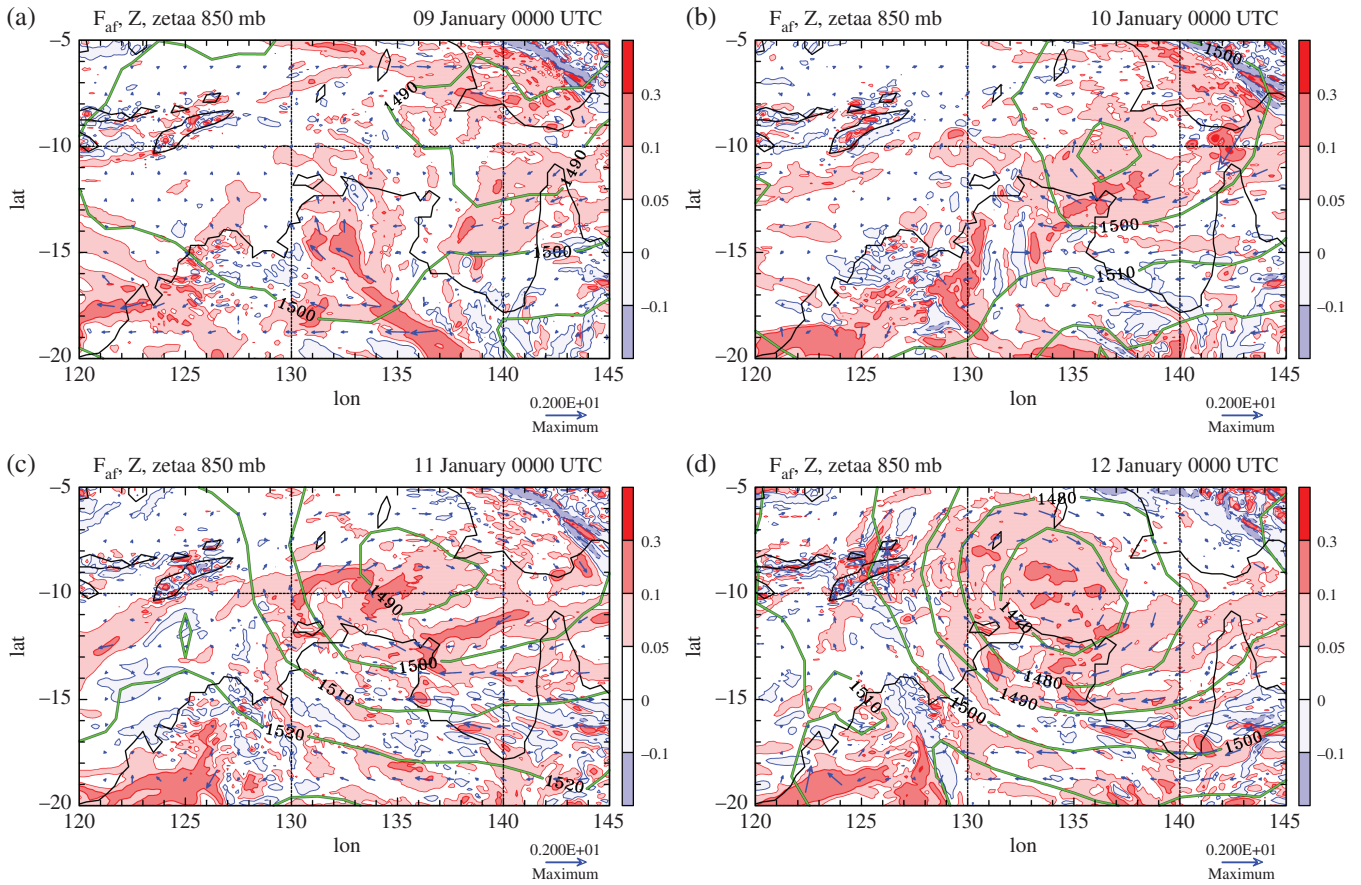

Figure 8. Vectors of the advective flux of absolute vorticity ($\mathbf{F}_{af}$) with contours of geopotential height (green, interval 10 m) and shaded contours of absolute vorticity, all at 850 mb at 0000 UTC from (a) 9 January to (d) 12 January 2014, illustrating the formation. Absolute vorticity shading is as shown on the label bar multiplied by 10^{-3} s^{-1}; cyclonic values of absolute vorticity are plotted as positive (red/pink), and anticyclonic values as negative (blue). Vectors of the advective flux of absolute vorticity (multiplied by 10^{-3}) should be compared to the reference vector (2 m s^{-2}) at the bottom right of each panel.

aggregation of regions of enhanced cyclonic vorticity overlapping with coherent regions of positive values of OW within the nascent vortex circulation are important elements of the marsupial paradigm.

5.3. *Moisture supply over land*

The focus of this section is to gain insight into how the low was able to intensify and persist over land in the absence of strong moisture fluxes from the ocean. Emanuel *et al.* (2008) suggested that the intensification of warm-core cyclones over land in Northern Australia can occur when the underlying soil is sufficiently warm and wet and the system is maintained by latent heat transfer from the soil. They state that 'when the storms are sufficiently isolated from their oceanic source of moisture, the rainfall they produce is insufficient to keep the soil wet enough to transfer significant quantities of heat, and the storms then decay rapidly'. The argument presented by Emanuel *et al.* (2008) is presumably influenced by the need for significant surface fluxes of moisture to give intensification in their model.

Recall from Figure 5 that, following landfall (at 0600 UTC on 14 January), the maximum wind speed increased following a continued reduction of the vertical wind shear. Figure 9 shows that after landfall the relative humidity and equivalent potential temperature averaged over a 2° column were higher. There was a large burst of convective activity within the 2° column just after landfall and some smaller bursts at later times, the most notable being apparent at 1200 UTC on 15 January. The average vertical mass flux over a 10° column suggests that convection was still occurring in the low, but not always near to the circulation centre. After landfall the circulation increased in strength around the 2° column, increasing in depth to around 400 mb until 17 January.

We examine now the moisture budget for a mesoscale column of air. The budget may be written as

$$\frac{\partial Q}{\partial t} = E - P + MC, \qquad (2)$$

where $\partial Q/\partial t$ is the change in TPW with time, E is the rate of evaporation of moisture from the surface, P is rate of moisture loss by precipitation and MC is the rate of moisture convergence. Precipitation and evaporation are variables available in the ECMWF forecast data, while moisture convergence is calculated by vertically integrating the fluxes of moisture into a column centred on the system. These three quantities are then averaged over the area of the column to provide units of kg s^{-1} m^{-2}.

Figure 11 shows sources and sinks of moisture obtained from Eq. (2) averaged over columns 2° × 2°, 4° × 4°, and 6° × 6° centred on the location of the minimum geopotential at 850 mb from 8 to 22 January. Shown also is the TPW averaged over the corresponding column. A key feature is that at most times the fluxes of moisture into the sides of the 2° column are equal to or larger than the amount of moisture lost by precipitation; the surface moisture fluxes make only a small contribution to the overall budget. A similar result has been found also for tropical cyclones (e.g. Kurihara, 1975; Braun, 2006; Trenberth *et al.*, 2007).

By itself, the availability of substantial column moisture does not mean that deep convection will occur or be sustained. Deep convection requires the presence of conditional instability and sustained deep convection requires that this instability be maintained. Thus, while surface moisture fluxes are a small component of the overall moisture budget, they are important in maintaining conditional instability in the central region of the vortex. This maintenance is important in supporting deep convection there, which is necessary for the intensification process. Indeed, Malkus and Riehl (1960) pointed out that a

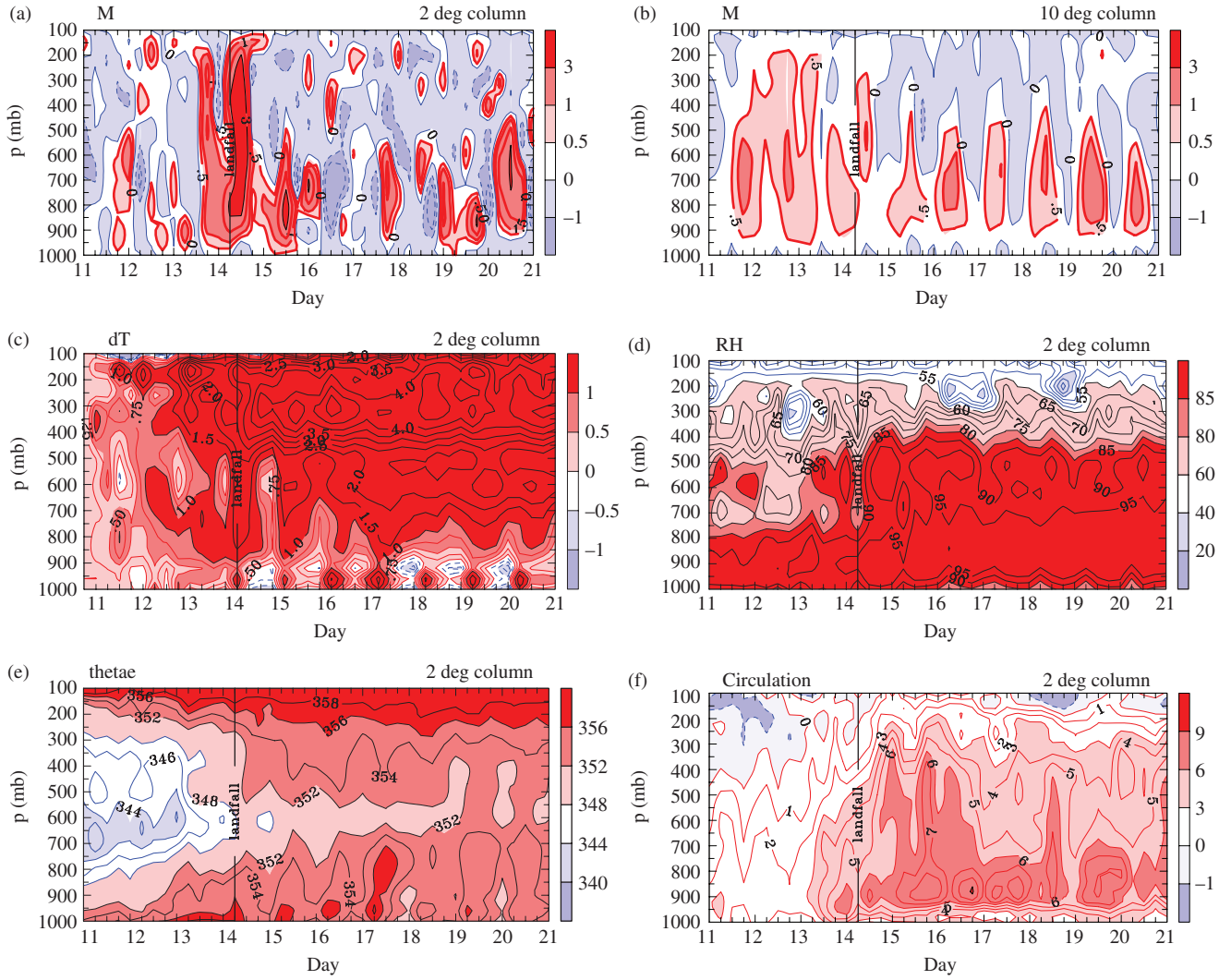

Figure 9. Time–height cross-sections of system-averaged quantities within a lat–lon columns (a, c–f) $2^\circ \times 2^\circ$ and (b) $10^\circ \times 10^\circ$, centred on the location of the minimum geopotential at 850 mb. These include (a,b) the vertical mass flux per unit area (kg m^{-2} s^{-1}), (c) the temperature deviation from that at the start of the time series, (d) the relative humidity (%), and (e) pseudo-equivalent potential temperature (K). (f) shows the normalized circulation (m s^{-1}) around the column.

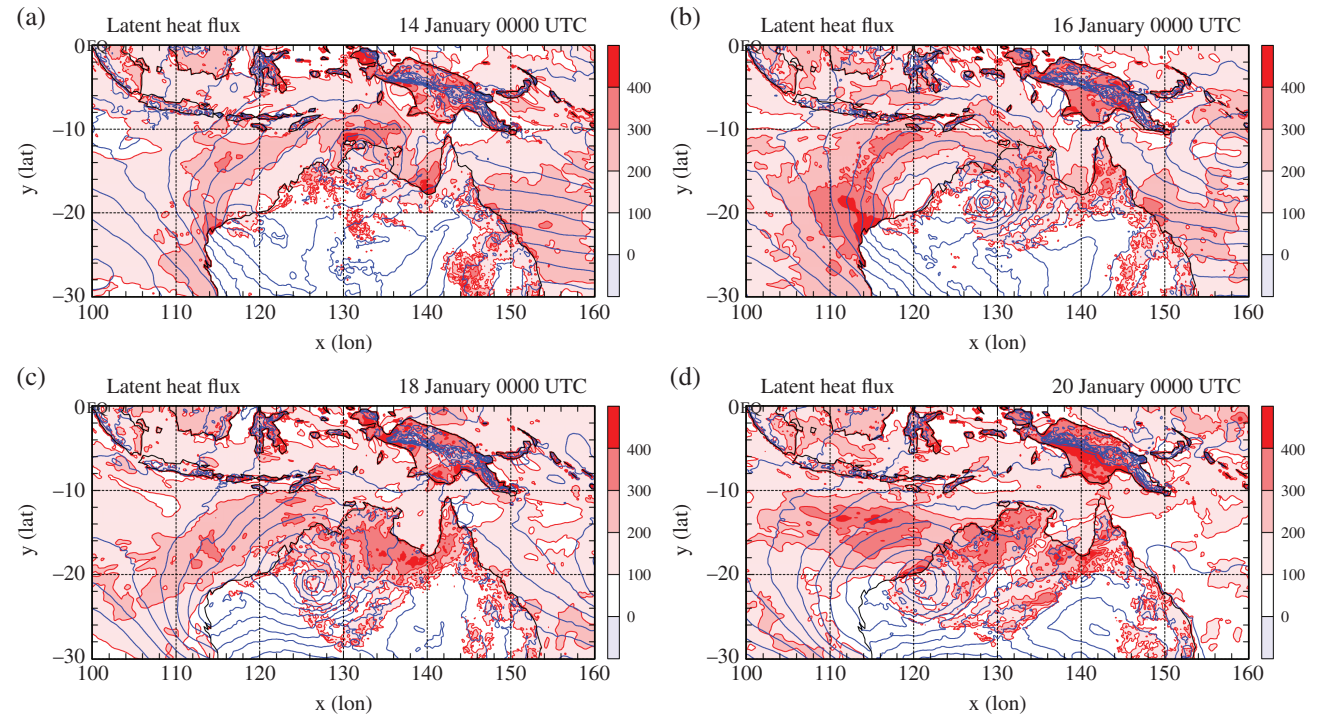

Figure 10. Exchange of latent heat with the surface through turbulent diffusion (shaded contours, W m^{-2}) and contours of geopotential height (blue, interval 10 m) for 0000 UTC on (a) 14, (b) 16, (c) 18 and (d) 20 January 2014.

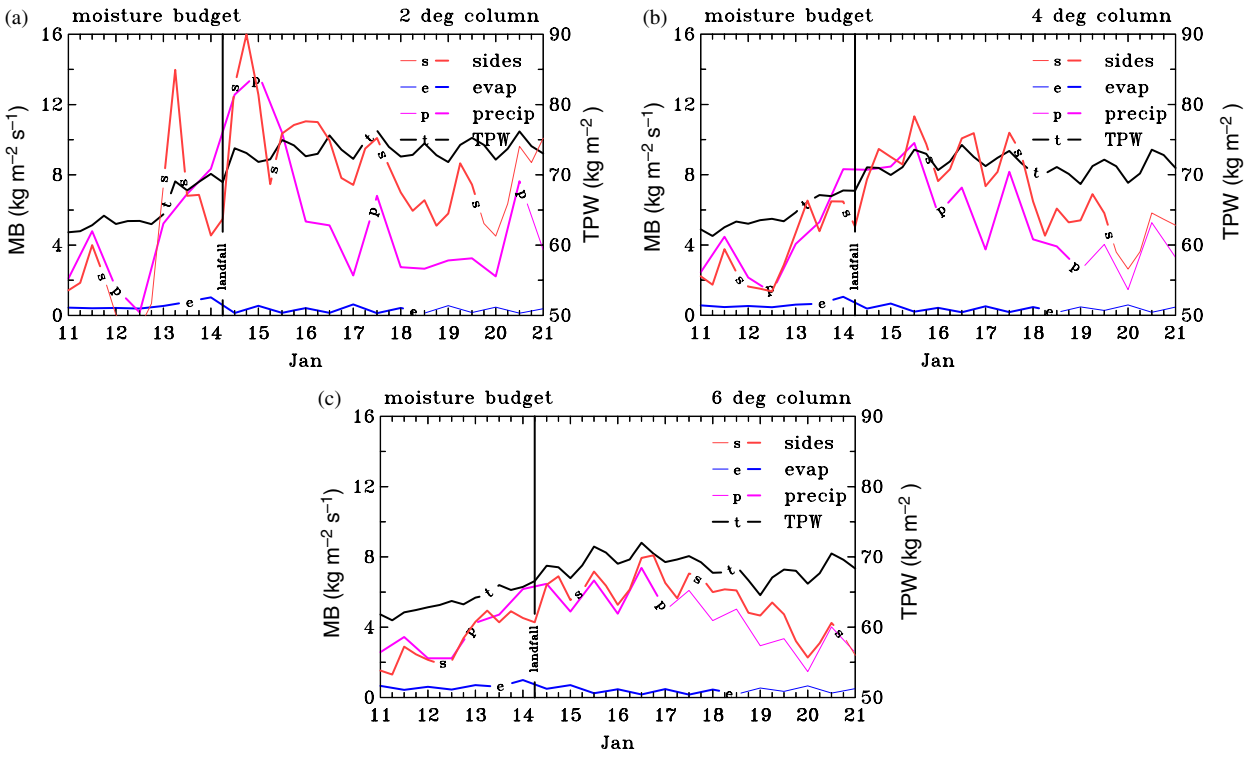

Figure 11. Sources and sinks of moisture including the contributions by surface evaporation, precipitation and the horizontal transport of moisture averaged over lat–lon columns (a) $2^\circ \times 2^\circ$, (b) $4^\circ \times 4^\circ$, and (c) $6^\circ \times 6^\circ$ centred on the location of the minimum geopotential at 850 mb. The horizontal transport of moisture is calculated by summing the vertically integrated fluxes of moisture into the column and then dividing the sum by the area of the column so that all terms have units $\mathrm{kg\,m^{-2}\,s^{-1}}$. The values shown here have been multiplied by 10^5. Also shown is the total precipitable water ($\mathrm{kg\,m^{-2}}$). A discussion of how the moisture budget is calculated and some issues about closure are found in section 5.3.

prerequisite for hurricanes to be able to form is an elevation of θ_e in the central region by surface moisture fluxes from the ocean.[‡‡] Figure 9(e) does show, *inter alia*, an increase in low-level θ_e averaged over the 2° column as the system develops, even while it is over land, suggesting that surface moisture fluxes are playing a role in the increase. As expected, after the low moves over land, the magnitude of the surface moisture fluxes decreases and a marked diurnal cycle becomes evident. This diurnal cycle is presumably a consequence of the daytime insolation over land.

A comparison of surface moisture fluxes over both land and sea is provided by Figure 10, which shows the patterns of the fluxes at 0000 UTC on 14, 16, 18 and 20 January. On 14 January the moisture fluxes are largest over the sea north of Darwin, while fluxes over the Australian continent are small (typically less than $100\,\mathrm{W\,m^{-2}}$). Two days later, when the low is further inland, there are somewhat enhanced moisture fluxes over land behind the low (there are regions with values between 300 and $400\,\mathrm{W\,m^{-2}}$) where there had been copious amounts of precipitation on the previous days (section 3). Over the next four days, there are enhanced fluxes over land behind the low. It is notable that large values of surface moisture fluxes occur regularly over Papua New Guinea indicating that significant moisture fluxes can occur over land if there is sufficient rainfall.

Returning to Figure 11, another feature worth noting is that the peak precipitation occurs between 14 and 16 January in the 2° column, corroborating the forecaster's analysis in section 3. In all columns, the TPW increases until about 16 January and then it remains approximately constant. Inspection of Figure 11 indicates that there is a period when the TPW remains approximately constant, even though the sum of terms on the right-hand side of Eq. (2) is positive. Apparently, the moisture budget is not closed, especially in the 2° column. The reasons for this may lie partly in the fact that water substance is not strictly a conserved quantity in many models (e.g. Braun, 2006), but also because the data available from the ECMWF system have certain deficiencies.[§§]

Figure 12 shows the visible geostationary satellite imagery at 0030 UTC on 12, 13, 14 and 15 January, half an hour later than the corresponding ECMWF analysis fields. To ascertain the ability of the ECMWF analysis to capture the observed location of organized convective regions, the vertical motion from the analyses at 500 mb and the geopotential at 850 mb are superimposed on the satellite imagery. At 0000 UTC on 12 January, the analysis shows several convective systems near the low, but there is essentially no convection in the vortex centre. Most of modelled regions of convective activity are overlapping or close to observed systems. The comparison at 0000 UTC on 13 January is similar, with the satellite observations confirming the lack of convective activity near the circulation centre. In particular, the banded cloud structures wrapping around the circulation centre in the visible imagery are captured qualitatively well by the model. However, the analysis has ascent north of the 'Top End', which is not observed. At 0000 UTC on 14 and 15 January, the model produces strong convection within the inner core of the system, consistent with the observations. These two times (0000 UTC on 14, 15 January) encompass the rapid intensification phase and there is generally a good match between regions of deep convection captured by the analyses and those observed. The foregoing comparisons give confidence that the analyses have adequate skill in reproducing the broadscale convective features that are observed.

In summary, we have shown that the horizontal transport of moisture into a column (for all box sizes analyzed here) following

[‡‡] Based on hydrostatic considerations alone, Malkus and Riehl estimated that for typical conditions in a hurricane, a fall in surface pressure of 1 mb would require an elevation of θ_e by 0.4 K.

[§§] There are many potential sources of error preventing closure in the moisture budget besides lack of conservation of total water. First, the precipitation and surface fluxes are not obtained from the analyses, but constructed from a time average of a 3 h forecast from the valid time. These forecasts data are available only at 12 h intervals. The foregoing precipitation and surface flux data are compared with the instantaneous moisture convergence into the moving column computed from the 6 h analysis data. Estimation of the translation speed of the column from 6 h analyses will introduce additional errors. Finally, TPW is calculated at 6 h intervals and calculation of its time tendency is subject to error also.

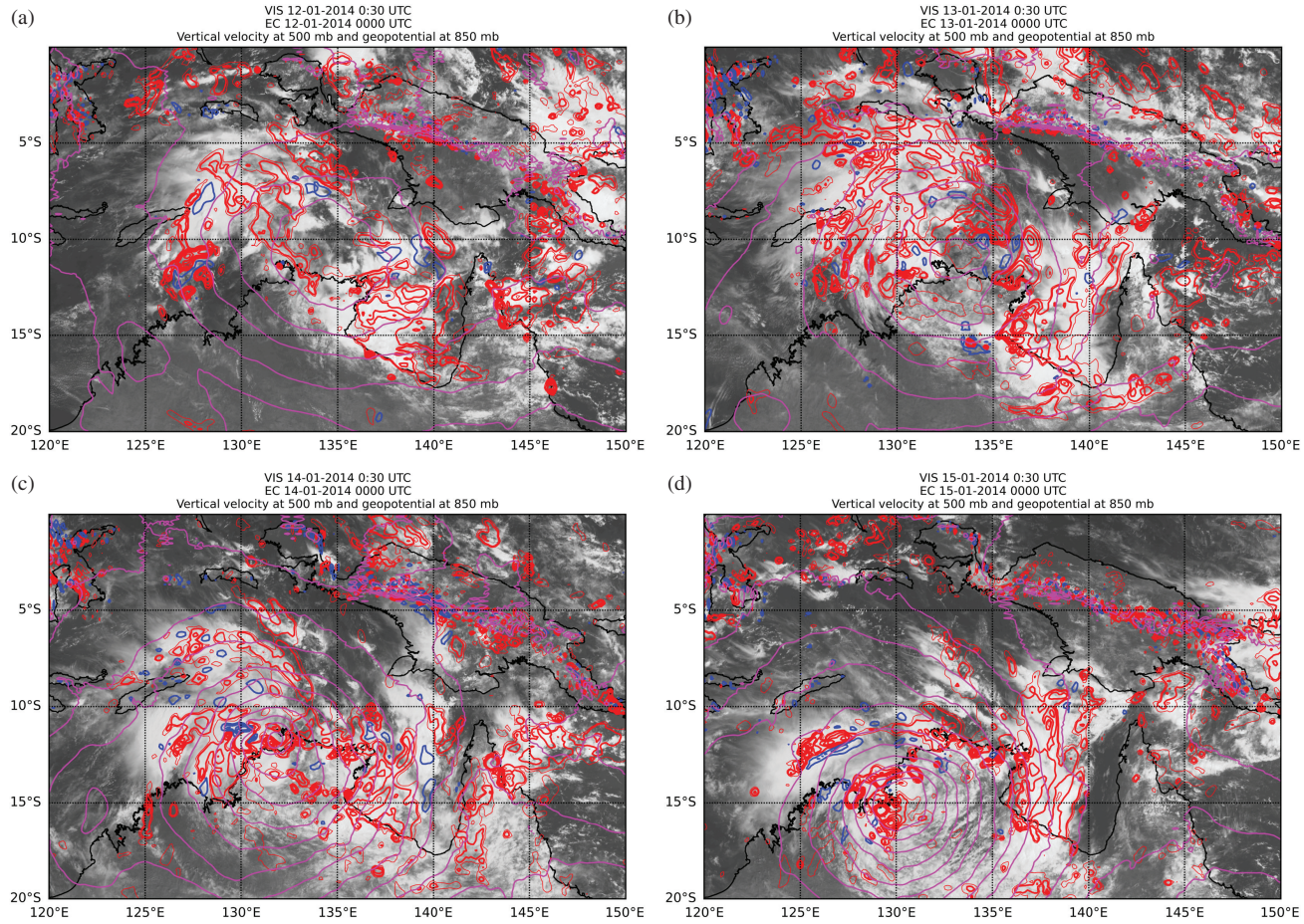

Figure 12. Visible satellite imagery from the MTSAT geostationary satellite half an hour after 0000 UTC on (a) 12 January, (b) 13 January, (c) 14 January and (d) 15 January 2014 with contours of vertical motion (ω) at 500 mb from the ECMWF analyses at the 0000 UTC times. Red contours denote upward motion ($\omega < 0$), blue contours subsidence. Thin red contours have intervals of 2.5×10^{-1} Pa s^{-1}, thick contours begin at 5×10^{-1} Pa s^{-1} and increase at intervals of 5×10^{-1} Pa s^{-1}. Shown also are contours of geopotential height (pink, interval 10 m).

the low is essentially equal to (or greater than) the moisture lost by precipitation. The contribution to the moisture budget by surface fluxes is small in comparison. Nevertheless, the small moisture fluxes play an important role in generating convective instability in a monsoon environment that already has relatively high values of TPW so that deep convective bursts can continue to occur even when the system is located far inland. The ECMWF analyses captured well the peak precipitation between 14 and 16 January, corroborating the forecaster's analysis in section 3.

6. Conclusions

We have presented an analysis of a tropical low that formed in the Australian monsoon in January 2014 and its subsequent intensification over land based on ECMWF analyses. Interpretations of the formation were given in terms of vorticity dynamics and related elements of the marsupial paradigm of tropical cyclogenesis. Support for the intensification was examined also from the perspective of a moisture budget. The analyses indicated that the intensification of the low required repeated bursts of deep convection near the centre of the gyre to promote the further concentration of same-sign vorticity near the centre. This concentration of vorticity increases the local circulation about the centre, which amounts to increasing the local tangential wind speed and, through approximate gradient wind balance above the boundary layer, to a lowering of the central pressure.

The low began to develop over water in moderate deep-layer shear, but in an environment with moderately high background vertical vorticity following two days of sustained convective bursts close to the circulation centre. These convective bursts moistened the mid- to upper-troposphere, increasing both the relative humidity and equivalent potential temperature at these levels as depicted by average conditions in a mesoscale (2°) column following the system. After the system made landfall, the horizontal transport of moisture into this column following the low is essentially equal to (or greater than) the moisture lost by precipitation, whereas surface moisture fluxes make only a small contribution to the overall budget. Nevertheless, enhanced surface moisture fluxes near the circulation centre play an important role in elevating moist equivalent potential temperature in the boundary layer, thereby supporting deep convection and, in turn, the intensification process.

The findings indicate that the processes of intensification are the same over land as those that operate over the ocean. All that is required is for deep convection to persist near the circulation centre, which requires an adequate import of moisture from the storm environment and a modest elevation of conditional instability near the storm centre to sustain deep convection there. There appears to be no need to invoke complex soil processes to explain intensification over land.

Acknowledgements

This work was motivated by a visit of the first three authors to the Australian Bureau of Meteorology's Regional Forecast Centre in Darwin during the monsoon season and the opportunity this visit provided to witness the monsoon first-hand as well as the forecasting challenges it poses. We thank Todd Smith for his warm hospitality and support for our research. We thank also the many forecasters at the Regional Office who have shared their expertise with us. We thank also Denis Margetic from the Bureau of Meteorology Head Office for supplying us with satellite data and for code to plot these data. We are grateful to two anonymous reviewers, whose perceptive and constructive comments helped to improve the manuscript. GK and RKS

acknowledges funding for tropical cyclone research from the German Research Council (Deutsche Forschungsgemeinschaft) under grant no. SM30/23-4 and the Office of Naval Research Global under grant no. N62909-15-1-N021. MTM acknowledges the support of NSF grant AGS-1313948, NOAA HFIP grant N0017315WR00048, NASA grant NNG11PK021 and the US Naval Postgraduate School.

References

Braun SA. 2006. High-resolution simulation of hurricane *Bonnie* (1968). Part II: Water budget. *J. Atmos. Sci.* **63**: 43–64.

Davidson NE. 2010. On the intensification and recurvature of tropical cyclone *Tracy* (1974). *Aust. Meteorol. Oceanogr. J.* **60**: 169–177.

DeMaria M, Kaplan J. 1994. A statistical Hurricane Intensity Prediction Scheme (SHIPS) for the Atlantic basin. *Weather and Forecasting* **9**: 209–220.

Dunkerton TJ, Montgomery MT, Wang Z. 2009. Tropical cyclogenesis in a tropical wave critical layer: Easterly waves. *Atmos. Chem. Phys.* **9**: 5587–5646.

Emanuel K. 1995. The behavior of a simple hurricane model using a convective scheme based on subcloud-layer entropy equilibrium. *J. Atmos. Sci.* **52**: 3959–3968.

Emanuel K, DesAutels C, Holloway C, Korty C. 2004. Environmental control of tropical cyclone intensity. *J. Atmos. Sci.* **61**: 843–858.

Emanuel K, Callaghan J, Otto P. 2008. A hypothesis for the redevelopment of warm-core cyclones over Northern Australia. *Mon. Weather Rev.* **136**: 3863–3872.

Evans C, Schumacher RS, Galarneau TJ Jr. 2011. Sensitivity in the overland reintensification of tropical cyclone *Erin* (2007) to near-surface soil moisture characteristics. *Mon. Weather Rev.* **139**: 3848–3870.

Haynes P, McIntyre ME. 1987. On the evolution of vorticity and potential vorticity in the presence of diabatic heating and frictional or other forces. *J. Atmos. Sci.* **44**: 828–841.

Kaplan J, DeMaria M. 1995. A simple empirical model for predicting the decay of tropical cyclone winds after landfall. *J. Appl. Meteorol.* **34**: 2499–2512.

Kilroy G, Smith RK. 2013. A numerical study of rotating convection during tropical cyclogenesis. *Q. J. R. Meteorol. Soc.* **139**: 1255–1269.

Kurihara Y. 1975. Budget analysis of a tropical cyclone simulated in an axisymmetric numerical model. *J. Atmos. Sci.* **32**: 25–59.

McBride JL, Keenan TD. 1982. Climatology of tropical cyclone genesis in the Australian region. *J. Clim.* **2**: 13–33.

Malkus JS, Riehl H. 1960. On the dynamics and energy transformations in steady-state hurricanes. *Tellus* **12**: 1–20.

Molinari J, Lombardo K, Vollaro D. 2007. Tropical cyclogenesis within an equatorial Rossby wave packet. *J. Atmos. Sci.* (Bruce Morton Memorial volume) **64**: 1301–1317.

Montgomery MT, Smith RK. 2014. Paradigms for tropical cyclone intensification. *Aust. Meteorol. Oceanogr. J.* **64**: 37–66.

Montgomery MT, Nguyen SV, Smith RK, Persing J. 2009. Is WISHE essential for tropical cyclone intensification? *Q. J. R. Meteorol. Soc.* **135**: 1697–1714.

Montgomery MT, Davis C, Dunkerton T, Wang Z, Velden C, Torn R, Majumdar SJ, Zhang F, Smith RK, Bosart L, Bell MM, Haase JS, Heymsfield A, Jensen J, Campos T, Boothe MA. 2012. The Pre-Depression Investigation of Cloud Systems in the Tropics (PREDICT) experiment: Scientific basis, new analysis tools and some first results. *Bull. Am. Meteorol. Soc.* **93**: 153–172.

Montgomery MT, Persing J, Smith RK. 2014. Putting to rest WISHE-ful misconceptions for tropical cyclone intensification. *J. Adv. Model. Earth Syst.* **7**: 92–109.

Raymond DJ, López Carillo C. 2011. The vorticity budget of developing typhoon *Nuri* (2008). *Atmos. Chem. Phys.* **11**: 147–163.

Raymond DJ, Gjorgjievska S, Sessions SL, Fuchs Z. 2014. Tropical cyclogenesis and mid-level vorticity. *Aust. Meteorol. Oceanogr. J.* **64**: 11–25.

Rozoff CM, Schubert WH, McNoldy BD, Kossin JP. 2006. Rapid filamentation zones in intense tropical cyclones. *J. Atmos. Sci.* **63**: 325–340.

Sharkov EA, Shramkov YN, Pokrovskaya IV. 2012. Increased water-vapor content in the atmosphere of tropical latitudes as a necessary condition for the genesis of tropical cyclones. *Izvestiya, Atmos. Oceanic Phys.* **48**: 900–908.

Shen W, Ginis I, Tuleya RE. 2002. A numerical investigation of land surface water on landfalling hurricanes. *J. Atmos. Sci* **59**: 789–802.

Smith RK, Montgomery MT. 2015. Towards clarity on understanding tropical cyclone intensification. *J. Atmos. Sci.* **72**: 3020–3031.

Smith RK, Montgomery MT, Kilroy G, Tang S, Müller SK. 2015. Tropical low formation during the Australian monsoon: The events of January. *Aust. Meteorol. Oceanogr. J.* **65**: 318–341.

Trenberth KE, Davis CA, Fasullo J. 2007. Water and energy budgets of hurricanes: Case studies of Ivan and Katrina. *J. Geophys. Res.* **112**: D23106, doi: 10.1029/2006JD008303.

Tory KJ, Kepert JD, Sippel JA, Nguyen CM. 2012. On the use of potential vorticity tendency equations for diagnosing atmospheric dynamics in numerical models. *J. Atmos. Sci.* **69**: 942–960.

